ENVIRONMENTAL RESEARCH
LETTERS

OPEN ACCESS

RECEIVED
11 October 2021

REVISED
11 April 2022

ACCEPTED FOR PUBLICATION
22 April 2022

PUBLISHED
13 May 2022

LETTER

Controls on the relative melt rates of debris-covered glacier surfaces

E S Miles[1,*], J F Steiner[2,3], P Buri[1,4], W W Immerzeel[2] and F Pellicciotti[1,5]

[1] Swiss Federal Research Institute WSL, Birmensdorf, Switzerland
[2] Department of Physical Geography, University of Utrecht, Utrecht, The Netherlands
[3] International Center for Integrated Mountain Development, Kathmandu, Nepal
[4] Geophysical Institute, University of Alaska Fairbanks, Fairbanks, AK, United States of America
[5] Department of Geography, University of Northumbria, Newcastle-upon-Tyne, United Kingdom
[*] Author to whom any correspondence should be addressed.

E-mail: evan.miles@wsl.ch

Keywords: debris-covered glacier, supraglacial debris, glacier ablation, surface energy balance, ice cliff, supraglacial pond, melt enhancement

Abstract

Supraglacial debris covers 7% of mountain glacier area globally and generally reduces glacier surface melt. Enhanced energy absorption at ice cliffs and supraglacial ponds scattered across the debris surface leads these features to contribute disproportionately to glacier-wide ablation. However, the degree to which cliffs and ponds actually increase melt rates remains unclear, as these features have only been studied in a detailed manner for selected locations, almost exclusively in High Mountain Asia. In this study we model the surface energy balance for debris-covered ice, ice cliffs, and supraglacial ponds with a set of automatic weather station records representing the global prevalence of debris-covered glacier ice. We generate 5000 random sets of values for physical parameters using probability distributions derived from literature, which we use to investigate relative melt rates and to isolate the melt responses of debris, cliffs and ponds to the site-specific meteorological forcing. Modelled sub-debris melt rates are primarily controlled by debris thickness and thermal conductivity. At a reference thickness of 0.1 m, sub-debris melt rates vary considerably, differing by up to a factor of four between sites, mainly attributable to air temperature differences. We find that melt rates for ice cliffs are consistently 2–3× the melt rate for clean glacier ice, but this melt enhancement decays with increasing clean ice melt rates. Energy absorption at supraglacial ponds is dominated by latent heat exchange and is therefore highly sensitive to wind speed and relative humidity, but is generally less than for clean ice. Our results provide reference melt enhancement factors for melt modelling of debris-covered glacier sites, globally, while highlighting the need for direct measurement of debris-covered glacier surface characteristics, physical parameters, and local meteorological conditions at a variety of sites around the world.

1. Introduction

Rocky debris covers the surface of approximately 7% of mountain glacier ice globally, but over 10% for some regions and frequently over 20% for individual glaciers, where it is concentrated in lower ablation areas (Scherler *et al* 2018, Herreid and Pellicciotti 2020). Due to difficulties in mapping debris-covered ice, as well as the melt-inhibiting effect of even moderate surface debris (e.g. Östrem 1959, Nicholson and Benn 2006), these glacier areas have been historically ignored in regional and global projections of glacier melt (e.g. Radić *et al* 2014, Huss and Hock 2015, Marzeion *et al* 2020). New debris thickness datasets offer promise for explicit representation of these areas in glacier models (Kraaijenbrink *et al* 2017, Compagno *et al* 2021, Rounce *et al* 2021), but the spatial variability of supraglacial debris thickness (McCarthy *et al* 2017, Nicholson *et al* 2018) and model parametric uncertainty pose considerable obstacles. Furthermore, bare ice exposures (i.e. ice cliffs) and supraglacial ponds are often scattered

across the surface of debris-covered glaciers (Steiner *et al* 2019, Kneib *et al* 2021a); these features are disproportionately responsible for these glaciers' mass loss (e.g. Immerzeel *et al* 2014, Pellicciotti *et al* 2015, Thompson *et al* 2016, Salerno *et al* 2017, Brun *et al* 2018, Miles *et al* 2018, Mölg *et al* 2019, Buri *et al* 2021) and are difficult to constrain due to their variability in space and time (Miles *et al* 2017a, Steiner *et al* 2019).

Detailed assessments of ice cliff melt rates and volume losses have been performed for select glaciers, almost exclusively in High Mountain Asia (Sakai *et al* 1998, 2002, Han *et al* 2010, Reid and Brock 2014, Steiner *et al* 2015, Brun *et al* 2016, 2018, Watson *et al* 2017b, Buri and Pellicciotti 2018, Anderson *et al* 2021, Mishra *et al* 2021, Stefaniak *et al* 2021). It is clear that ice cliff geometry is a key control on their melt rates: they experience differential melt rates based on their aspect (Sakai *et al* 2002, Buri and Pellicciotti 2018), and their steep surface complicates their radiative budget (Han *et al* 2010, Steiner *et al* 2015). In addition, ice cliffs' low albedo (Sakai *et al* 1998, Steiner *et al* 2015, Watson *et al* 2017b) is likely to enhance their energy receipts and melt rates relative to debris-free glacier ice. Ice cliffs' steep slopes additionally increase their true surface area, often by up to 40% (Anderson *et al* 2021), further increasing their melt contributions.

The complex dynamics of supraglacial ponds (Röhl 2008, Benn *et al* 2012, Xin *et al* 2012, Watson *et al* 2016, 2017a, Miles *et al* 2017a, 2017c, Steiner *et al* 2019) make it challenging to assess their role at the glacier scale (Salerno *et al* 2017, Miles *et al* 2018). These features generally have a positive surface energy balance and contribute to local ablation at the glacier surface (Benn *et al* 2001, Röhl 2006, Miles *et al* 2016, Salerno *et al* 2017), but their primary contribution to glacier ablation is the dissipation of absorbed energy to the glacier's interior when they drain (Sakai *et al* 2000, Benn *et al* 2012, Miles *et al* 2016, 2018).

Several cliff and pond studies have assessed a melt enhancement factor for these features relative to the general rate of glacier ablation beneath the surrounding surface debris (Sakai *et al* 2002, Immerzeel *et al* 2014, Brun *et al* 2018, Miles *et al* 2018, Mishra *et al* 2021), enabling a basic representation of these features in regional glacier melt models (Kraaijenbrink *et al* 2017). This pragmatic approach is to-date hampered by the limited geographic representativeness of the few field observations and the use of sub-debris melt as a reference rate. To progress with understanding of mass losses for debris-covered glaciers, there is a need for an assessment of the melt rates of debris-covered glacier surfaces considering the geographic and climatic domains where surface debris is widespread. We hypothesize that the melt enhancement of ice cliffs and supraglacial ponds is highly variable due to differences in reference sub-debris melt rates, but that differences in melt rates can be related directly to local meteorological conditions.

We aim to address two key questions:

(a) How do the melt rates of ice cliffs and supraglacial ponds compare to sub-debris and bare ice melt rates across different climates?
(b) Which physical parameters and meteorological conditions drive the heterogeneity of melt enhancement factors for debris, ice cliffs, and supraglacial ponds relative to clean ice?

To address these questions, we model the surface energy balance and associated melt rates for clean ice, debris-covered ice, ice cliffs, and supraglacial ponds using meteorological information from Automatic Weather Stations (AWSs) at debris-covered glacier sites around the world.

2. Methods

We compiled the most recent and complete AWS meteorological datasets available for each region. Our approach required a suite of high-quality meteorological observations encompassing much of an ablation season, which varies by site, in order to provide accurate forcing for our models and to ensure that the results are representative for real debris-covered glacier domains. Specifically, we required that stations include observations of downwelling measurements for both shortwave and longwave radiation, near-surface air temperature and relative humidity, and wind speed. These criteria enabled us to identify 13 sites covering a range of geographic and climatic conditions (figure 1; table 1). The available stations cover most regions of the Randolph Glacier Inventory (RGI, Pfeffer *et al* 2014) representing nearly all areas with considerable surface debris (Scherler *et al* 2018) and spanning the majority of the climatic envelope of debris-covered glacier sites (figure 1, right).

Using these data, our analysis aimed to calculate the melt rate for each surface type as if it were located exactly at the AWS location. We note that meteorological conditions and surface melt of course vary considerably across a single glacier, let alone regionally or globally. Our aim here is simply to ensure that the diversity of meteorological forcing where supraglacial debris is found globally is represented in our analysis, and to examine the effect of these conditions on glacier surface melt rates. We note that supraglacial ponds, ice cliffs, and debris-covered ice are indeed present at all the sites investigated.

We apply models of surface energy balance for debris-covered ice (Steiner *et al* 2021), ice cliffs (Buri *et al* 2016), and supraglacial ponds (Miles *et al* 2018), and also model the energy balance of bare glacier ice (Reid *et al* 2012) as a reference (see appendix). We model these distinct surface types for periods

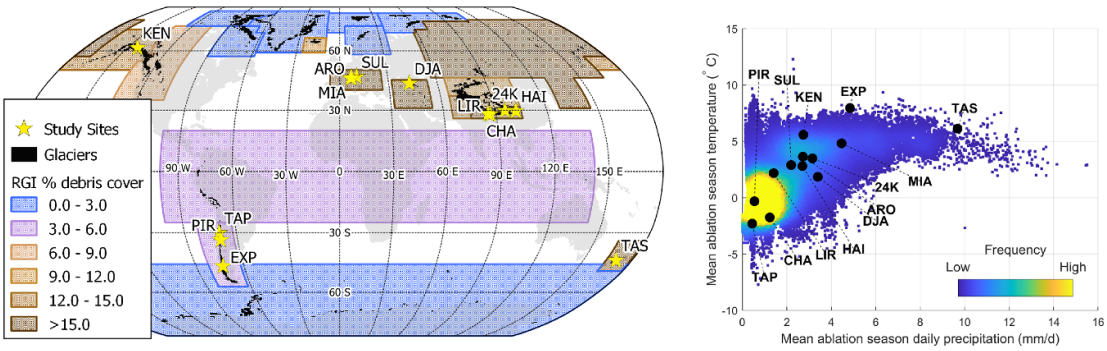

Figure 1. The 13 glaciers studied in this analysis cover nearly all regions of the Randolph Glacier Inventory (RGI) (Pfeffer *et al* 2014) which exhibit considerable surface debris (Herreid and Pellicciotti 2020) (left). These 13 sites also occupy very distinct climatic settings but are representative for the global climatic envelope of debris-covered ice (right), here evidenced by ablation season mean temperature and precipitation derived from WorldClim 2.1 (Fick and Hijmans 2017) for all pixels containing debris-covered ice. Glacier labels: 24K—24K, ARO—Arolla, CNU—Changri Nup, DJA—Djankuat, EXP—Exploradores, HAI—Hailuogou, KEN—Kennicott, LIR—Lirung, MIA—Miage, PIR—Piramide, SUL—Suldenferner, TAP—Tapado, TAS—Tasman.

where the WorldClim 2.1 (Fick and Hijmans 2017) monthly maximum air temperature is above 0 °C at the station's location, in order to compare only periods that are definitely within the local ablation season. It is worth noting that presence or absence of supraglacial debris alters lapse rates of near-surface air temperature (Steiner and Pellicciotti 2016, Shaw *et al* 2017) and that although turbulent fluxes differ over debris due to surface characteristics (Steiner *et al* 2018), similarity theory is equally applicable for clean and debris-covered ice (Nicholson and Stiperski 2020). The energy balance models for supraglacial ponds and ice cliffs have been developed based on meteorological data collected over debris, as in this study.

These four energy-balance models (debris, cliff, pond, clean) require specification of numerous physical parameters and characteristics (see appendix), which are constrained for only selected sites globally (e.g. Nicholson and Benn 2012, Rounce *et al* 2021). We thus prescribed conservative probability distributions for each parameter from the available literature, and determined 5000 independent, random parameter sets for each model (table 2). This Monte Carlo approach enabled us to ignore real differences in cliff, pond, and debris characteristics between sites, as we lack parameter estimates from each site, and to instead focus on the energy balance responses of each surface to distinct meteorological forcing. This allowed a comprehensive representation of all possible geometric and meteorological scenarios for each surface and site, therefore overcoming the potential bias of past studies that have investigated selected features in detail. Based on the 5000 Monte Carlo parameter sets, we determined functional relationships between debris thickness and sub-debris melt (Östrem 1959) at each site by fitting a first-order rational expression (Anderson and Anderson 2016). We also produced distributions of melt rates for ice cliffs, supraglacial ponds, and clean ice (figures 2 and 3).

We analysed the probabilistic melt rates to assess the relative melt rates compared to sub-debris melt rates at the 13 AWS locations. Specifically, we first examined the ratio of melt of cliff, pond, and clean ice surfaces to the sub-debris melt rate at each site. This ratio yielded a factor comparable to the melt 'enhancement factor' reported by past studies as a metric of the faster melt at ice cliffs compared to the surrounding debris (Sakai *et al* 2002, Immerzeel *et al* 2014, Brun *et al* 2018, Miles *et al* 2018, Buri *et al* 2021). We additionally calculated the ratio of cliff, pond, and sub-debris melt to clean glacier ice melt to provide an alternative enhancement factor unbiased by debris thickness, as in Rounce *et al* (2021). In these calculations we considered the full set of simulation results for each surface to produce probabilistic enhancement factors.

We then analysed the meteorological and parametric drivers of each surface's melt rate and enhancement factor variability. We first determined the mean value of key meteorological variables at each site for its model period, then related these meteorological characteristics to the variations of each surface's melt rates and enhancement factors across sites. We additionally correlated the melt rates at each site to each individual physical parameter (table 2) to assess which are most vital to constrain with field measurements, enabling us to compare the meteorological and parametric sensitivities for each surface.

3. Results

3.1. Probabilistic melt rates of debris, cliffs, ponds, and clean ice

Our results show a wide variety of melt rates (figure 2, table 3). For sub-debris melt rates, the parametric variability appears much greater than the variability

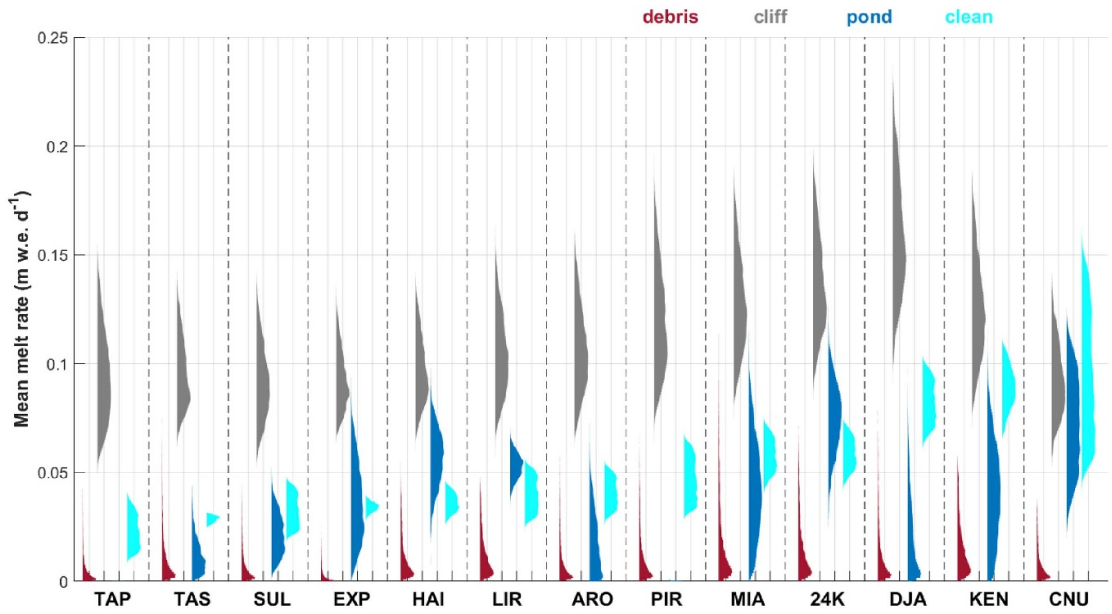

Figure 2. Distribution of mean ablation season melt rates modelled at each site. Sites are ordered by the median modelled clean ice melt rate. Glacier labels: TAP—Tapado, PIR—Piramide, EXP—Exploradores, ARO—Arolla, MIA—Miage, SUL—Suldenferner, DJA—Djankuat, KEN—Kennicott, LIR—Lirung, CNU—Changri Nup, 24K—24K, HAI—Hailuogou, TAS—Tasman.

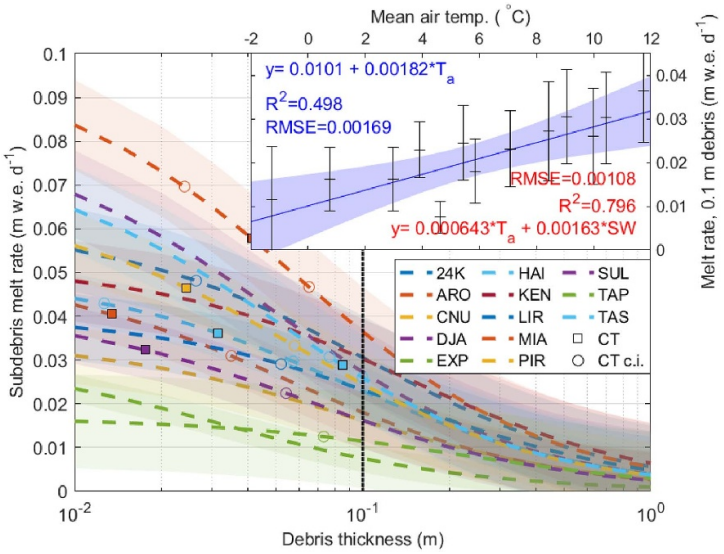

Figure 3. Østrem curves for the 13 study glaciers displayed as rational fits to the 5000 results for each site, along with shaded 95% confidence intervals (see SuppMat for full results, fit parameters, and alternative fit types). Also shown are critical debris thicknesses (CT) and their confidence intervals (CT c.i.) where applicable. Air temperature and shortwave radiation together explain 80% of the variability in melt rates between sites for a 0.1 m debris layer. Glacier labels: 24K—24K, ARO—Arolla, CNU—Changri Nup, DJA—Djankuat, EXP—Exploradores, HAI—Hailuogou, KEN—Kennicott, LIR—Lirung, MIA—Miage, PIR—Piramide, SUL—Suldenferner, TAP—Tapado, TAS—Tasman.

between sites, leading to more than an order of magnitude of variation for each site, but mean sub-debris melt rates are below 0.02 m w.e. d^{-1} at all sites. Only a few sites exhibit melt rates up to 0.05 w.e. m d^{-1} for thin debris (24K, KEN, MIA, TAS).

Ice cliff melt rates also show considerable parametric variability, varying by a factor of two at most sites. This roughly parallels the magnitude of variation between sites, with mean melt rates falling between 0.09 (CNU, SUL) and 0.16 (DJA) m w.e. d^{-1}. Ice cliffs exhibit the highest melt rates of any surface for all sites except CNU, where the distribution of ice cliff melt rates broadly overlaps with the distributions for supraglacial ponds and clean ice.

The mean supraglacial pond net energy balance (hereafter expressed as a mean melt rate) is much more variable between sites, and also varies in parametric sensitivity between sites. At PIR and TAP, the seasonal energy balance is negative for nearly all simulations, indicating overriding evaporation

irrespective of parameter choice. At 24K and CNU, on the other hand, mean melt rates exceed 0.07 m w.e. d^{-1}. Pond mean melt rates exhibit very high parametric spread for some sites (CNU, EXP, KEN, MIA) and very tight distributions for others (LIR, TAS, SUL).

Modelled clean ice melt rates vary considerably between sites, from 0.02 m w.e. d^{-1} at TAP to 0.09 m d^{-1} at KEN and CNU. As the physically-meaningful parameter space for this model is better constrained than for the other surfaces, modelled melt rates for most sites exhibit a fairly tight spread, with the exception of CNU. Conversely, TAS and EXP exhibit a considerably tighter spread of modelled melt rates, despite showing lower mean modelled melt rates than at many sites.

3.2. Sub-debris melt and controls

As has been demonstrated previously (Östrem 1959, Rounce *et al* 2021), the presence of surface debris lowers ice melt rates relative to a clean glacier surface. Considering our hypothetical debris thickness distribution (which has a median thickness of 0.5 m), this leads to between 25× and 4× melt reduction on average. All sites show a strong reduction of melt rates with increasing debris thicknesses (figure 3), and our results indicate that debris thickness explains on average 67% of the variability in melt rates at a given site. The 95% confidence interval for our rational fit reaches 0 m d^{-1} for all sites between 1 and 2 m debris thickness, but modelled melt rates diverge sharply for thinner debris. Thermal conductivity (k_d) also exerts statistical control over sub-debris melt rates (mean p-value < 0.001) and explains 8% of the melt rate variance for each site. z_{0_d} plays a role for sub-debris melt rates at some sites (mean p-values 0.03) but explains <1% of the melt rate variance (figure 6).

Considering a thickness of 0.1 m, our sub-debris melt rate results indicate a spread of 4× between sites based on meteorological conditions alone (figure 3). This inter-site variability dwarfs the parametric variability of melt rates for all debris parameters other than thickness. Our results indicate that the differences in sub-debris melt rates between sites are strongly correlated with differences in mean air temperature and mean downwelling shortwave radiation (figure 3 inset), which together account for 80% (50% for T_a alone) of the difference in sub-debris melt rates between sites for 0.1 m debris thickness, as for clean ice (Braithwaite 1981). Notably, however, we did not find a clear association between site-specific meteorology and the sub-debris melt rate enhancement relative to a clean ice surface.

Since we determine the energy balance of debris-covered and clean ice glacier surfaces in parallel, we can leverage our results to consider, for each site, the critical debris thickness where sub-debris melt equates to the melt of a debris-free surface (Reznichenko *et al* 2010). In theory, at this thickness the increase in energy receipts due to low debris surface albedo is compensated by the reduced efficiency of conduction through thicker debris, but more recent work has highlighted that this effect may only occur in specific meteorological conditions (Evatt *et al* 2015) or not at all (Fyffe *et al* 2020). Our results indicate that at only six of 13 sites is the median clean ice melt rate equalled at a debris thickness on our Østrem curve, generally <4 cm but 8.5 cm at TAS (appendix). Three (ten) sites exhibited critical thicknesses for the 0.025 (0.975) confidence level. HAI, MIA and TAS exhibited critical thicknesses for the full confidence interval, while CNU, EXP and KEN did not exhibit a critical debris thickness above 0.01 m (the lower limit of our debris thickness parameter distribution) even at the 0.975 confidence level.

3.3. Melt enhancement factors for ice cliffs and supraglacial ponds

Directly comparing the model results, we determine enhancement factors normalised to sub-debris and clean-ice melt (figure 4). Cliffs and ponds exhibit high enhancement factors relative to debris-covered ice (2–30× higher) for all sites, with the exception of the pond energy balance at PIR and TAP. However, the enhancement factor spread in all instances is nearly an order of magnitude due to the variable debris thickness and its strong influence on sub-debris melt rates. Here, as we have maintained the theoretical parameter distributions between sites, the debris thicknesses do not match actual values at each site, so our enhancement factors do not entirely align with past studies leveraging, for example, geodetic mass balances (e.g. Immerzeel *et al* 2014, Brun *et al* 2018, Mishra *et al* 2021). However, our results are broadly in line with suggestions that cliffs and ponds enhance melt by a factor of roughly 10–20 relative to thick debris-covered areas (e.g. Sakai *et al* 2002, Immerzeel *et al* 2014, Miles *et al* 2018, Buri *et al* 2021), while cliffs and ponds enhance melt less where debris is generally thinner and sub-debris melt rates are higher (Brun *et al* 2018, Anderson *et al* 2021). We note that ice cliffs enhance melt more than ponds at all 13 sites considering equal planimetric areas.

Considering enhancement factors relative to a clean ice surface is more useful from a modelling perspective (Rounce *et al* 2021), and also reduces the apparent enhancement factor spread due to debris thickness variability. From this perspective (figure 4), it becomes clear that ice cliffs generally melt at rates 2-3 times higher than a clean glacier ice surface. Ponds, on the other hand, still show highly variable enhancement factors, and some sites are considerably more uncertain due to parametric factors. Notably, our results show that ponds are nearly as efficient as cliffs in absorbing atmospheric energy at

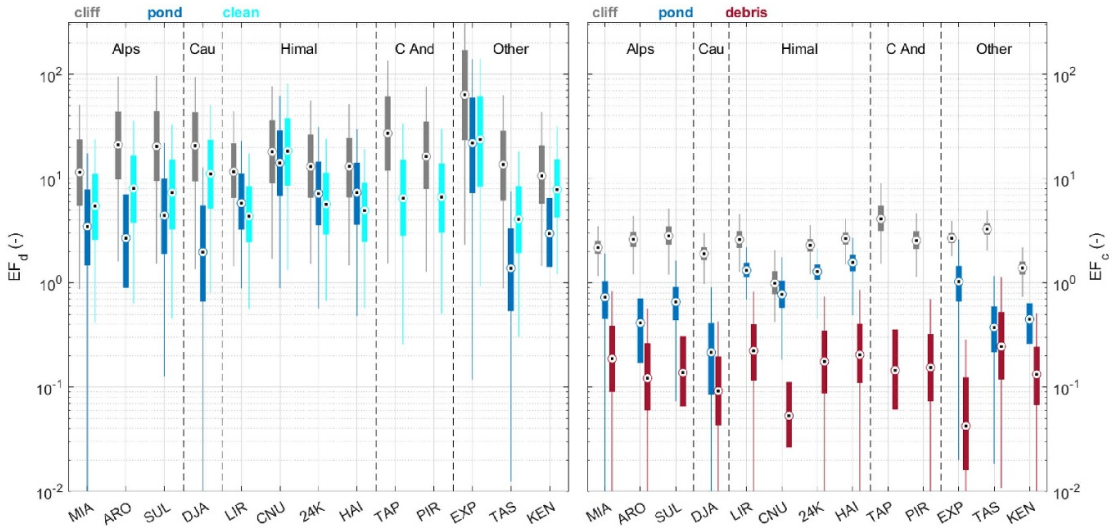

Figure 4. Enhancement factors relative to sub-debris (EF_d, left) and clean-ice (EF_c, right) melt rates show regional patterns due to meteorological similarities. Glaciers are grouped by mountain range: Cau—Caucasus, Himal—Himalaya, C And—Central Andes. Glacier labels: TAP—Tapado, PIR—Piramide, EXP—Exploradores, ARO—Arolla, MIA—Miage, SUL—Suldenferner, DJA—Djankuat, KEN—Kennicott, LIR—Lirung, CNU—Changri Nup, 24K—24K, HAI—Hailuogou, TAS—Tasman.

sites in the Himalayas (LIR, CNU, 24K, HAI), but are much less efficient in all other locations. However, it is also crucial to note that not all energy absorbed by ponds will lead to glacier ablation; pond seasonal drainage and freezing must be accounted for (Miles *et al* 2017a, 2018).

3.4. Parametric and meteorological controls on ice cliff melt

As for sub-debris melt, differences in ice cliff melt rates between sites are most clearly associated to differences in air temperature ($p = 0.024$, Pearson's $r = 0.62$; figure 6). As for clean glacier ice, although shortwave radiation is the single largest energy flux, variations in melt rates between locations are primarily controlled by differences in turbulent fluxes, for which air temperature is a good proxy (Braithwaite 1981). Our results indicate that sky-view factors ($V_{s,I}$ and $V_{s,L}$) and surface slope (β_i) are controls of ice cliff melt rates at all sites (mean p-values < 0.001, $\ll 0.001$, and 0.01, respectively). Of these, $V_{s,L}$ and β_i help to explain the variance between model realizations (38% and 6%, respectively). Ice cliff aspect (ψ_i) varies in importance between sites but explains on average 22% of the melt rate variance for a given site (figure 6). Investigations at individual sites have previously demonstrated that moderate aspect differences in fact dramatically alter ice cliff evolution (Sakai *et al* 2002, Buri and Pellicciotti 2018).

The enhancement factor for ice cliffs relative to clean ice is also not directly associated to specific meteorological conditions, but is inversely correlated with clean ice melt rates themselves (figure 5). That is, clean ice melt rates are driven in different settings by distinct ablation regimes resulting from the interaction of air temperature and incident radiation (Hock 2005, Pellicciotti *et al* 2005), and all of these conditions affect ice cliff melt rates as well, with cliffs enhancing melt relative to clean glacier ice in all settings. The extra energy absorption of ice cliffs due to their low albedo represents a progressively smaller portion of the net energy balance as clean ice melt rates increase. Although the ice cliff melt enhancement appears to decrease linearly (figure 5, $R^2 = 0.846$), an exponential decay converging on parity with clean ice melt is more physically justified and explains slightly more of the variance in our results ($R^2 = 0.881$), also providing a straightforward implementation in glacier melt models.

3.5. Parametric and meteorological controls on supraglacial pond energy balance

Our results indicate that differences in supraglacial pond energy receipts are closely related to turbulent fluxes differences, both at individual sites and between sites. For any given site, only the water surface temperature estimation parameters ($T_{ws,0}$, $T_{ws,m}$) meaningfully control the supraglacial pond melt rates (mean p-values $\ll 0.001$) explaining on average 51% and 32% of the net energy balance variance, respectively (figure 6). Meanwhile, the variations in pond melt rates between sites are strongly associated with variations in relative humidity ($p = 0.005$, Pearson's $r = 0.722$) and wind speed ($p = 0.005$, Pearson's $r = -0.722$), and these meteorological variables also control variations in the ponds' enhancement factor relative to clean ice (figure 5). Turbulent fluxes have

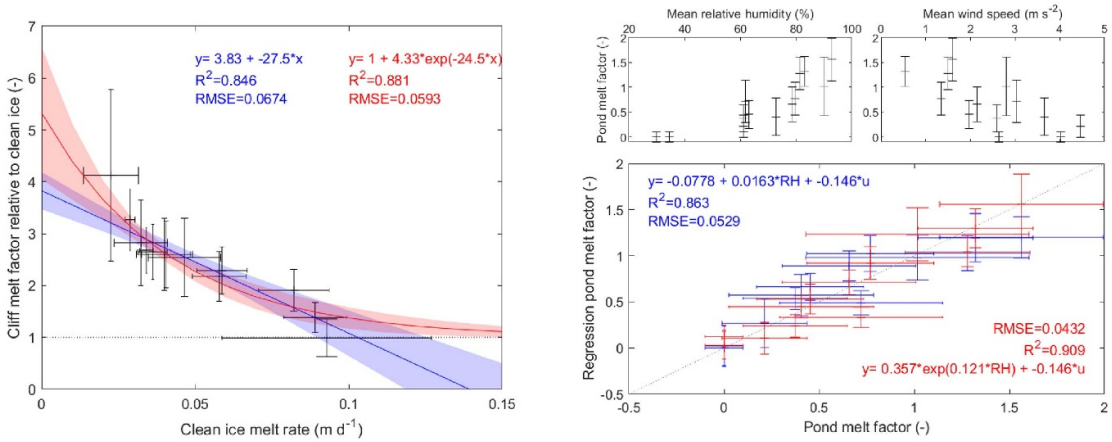

Figure 5. Ice cliff enhancement factors (left) are closely related to clean ice melt rates, and show decreasing cliff melt enhancement with increasing clean ice melt rates. Pond enhancement factors (right) are represented well by relative humidity and wind speed, as their energy balance is dominated by latent energy exchange; a non-linear model (red) only slightly outperforms a linear model (blue).

previously been shown to be an important energy flux for turbid supraglacial ponds in the Central Himalaya (Sakai *et al* 2000, Miles *et al* 2016), and these results extend that finding to show that they are equally important globally, with contrasting outcomes in terms of pond energy balance.

4. Discussion

4.1. Importance of cliffs and ponds

Studies have shown that ice cliffs and supraglacial ponds can considerably enhance local and glacier-wide overall melt rates for debris-covered glaciers (Benn *et al* 2001, Sakai *et al* 2002, Thompson *et al* 2016, Salerno *et al* 2017, Miles *et al* 2018, Buri *et al* 2021). However, these features typically account for less than 15% of the glacier's debris-covered area (e.g. Steiner *et al* 2019, Anderson *et al* 2021, Falaschi *et al* 2021, Kneib *et al* 2021a), and recent work has demonstrated that this melt enhancement is therefore not likely to fully compensate for the melt-reducing effects of supraglacial debris (Brun *et al* 2018, Anderson *et al* 2021, Rounce *et al* 2021).

Our results provide several key pieces of information to this area of inquiry. First, we show that ice cliffs indeed melt at an enhanced rate for the entire climatic range of supraglacial debris, At the sites we have analysed, ice cliffs melt at 2–3 times the rate of clean glacier ice and up to 20 times the rate of debris-covered ice (depending on the debris thickness). These are higher values than previously accounted for but certainly insufficient to bring melt rates for debris-covered areas to parity with clean ice in the same setting (Brun *et al* 2018, Anderson *et al* 2021, Rounce *et al* 2021). We also note that the turbid supraglacial ponds typical of debris-covered glaciers absorb energy less quickly than clean glacier ice in most settings that we studied. Consequently our results support the conclusion that debris thickness patterns dominate the mass balance pattern of debris-covered glaciers, while surface features provide heterogeneity and amplify the overall melt rate in varying degrees (Anderson *et al* 2021).

Nonetheless, these features' ability to moderate local and glacier-scale melt underlines the importance of accounting for them carefully in glacier- and regional-scale models of mass balance and evolution. We note that melt due to cliffs and ponds is included in geodetic mass balance measurements, so glacier model calibration to these measurements implicitly represents these features (Compagno *et al* 2021, Rounce *et al* 2021), but in a static manner that may not always represent their feedbacks to glacier evolution (Ferguson and Vieli 2021, Rowan *et al* 2021). Crucially, however, supraglacial ponds and cliffs are known to vary at seasonal and decadal timescales (Gardelle *et al* 2011, Benn *et al* 2012, Watson *et al* 2016, Miles *et al* 2017c, Mölg *et al* 2019, Steiner *et al* 2019, Mishra *et al* 2021, Kneib *et al* 2021b), necessitating an understanding and representation of how these features and their distribution will change in time and highlighting the need to develop spatial distributions of debris-covered ice facies. Considerable progress has been achieved in this direction in recent years through direct mapping of features and through association of topographic metrics (Herreid and Pellicciotti 2018, Watson *et al* 2018, King *et al* 2020, Anderson *et al* 2021, Kneib *et al* 2021a), and our results inform the next generation of glacier models to use such results to account for ice cliff and sub-debris melt.

4.2. Priorities for new measurements

In this study we used on-debris meteorological measurements to infer the primary meteorological and

parametric controls of distinct surfaces' melt rates. We sourced data exclusively from meteorological stations positioned over supraglacial debris, and our selection of sites roughly spans the climatic conditions of supraglacial debris, but for some regions no suitable data were available to us. We were unable to identify suitable on-debris AWS records for the Low Latitudes, Western Canada and US, Greenland, and Iceland, regions where debris covers a moderate portion of glacial area. Similarly, no suitable meteorological records were available for South Asia West, Central Asia, and Svalbard. Very little supraglacial debris is present for the Antarctic Periphery, Arctic Canada, the Russian Arctic, Scandinavia, and North Asia (Scherler *et al* 2018, Herreid and Pellicciotti 2020); these regions are not represented in our study. Several other sites could be analysed for South Asia East and we opted to include four sites within this region. Although large-scale modelling studies have demonstrated the utility of distributed climate reanalysis datasets, the use of high precision on-glacier meteorological observations provides an important foundation to test and evaluate energy balance models. In this respect, the geographical distribution of sites in this study highlights the need for new observations in underrepresented areas where supraglacial debris is prevalent.

A key question relating to debris-covered glaciers relates to overall melt reduction or increase in the debris-covered area (Rounce *et al* 2021). At the local and glacier scale this depends heavily on debris thickness, but debris thickness remains poorly constrained globally. Rounce *et al* (2021) have produced the first global maps of debris thickness and sub-debris enhancement factors, opening the possibility of representing sub-debris melt within large-scale models. However, the large parametric uncertainties underlying current data products may limit the utility of such datasets for projecting future melt. To reduce modelled debris thickness uncertainties, though, new methods are needed to constrain other debris properties. Furthermore, due to temporal discrepancies between the underlying global supraglacial debris area (Scherler *et al* 2018) and the Randolph Glacier Inventory (RGI, Pfeffer *et al* 2014), this dataset does not always represent debris-covered areas well (Herreid and Pellicciotti 2020). Regarding our sites, for example, the debris-covered area of Tapado Glacier is not represented within the RGI (or, therefore, the Scherler *et al* (2018) or Rounce *et al* (2021) products), although this complex debris-rich composite glacier landform is well-known (Pourrier *et al* 2014). Future efforts are needed to provide date-consistent glacier extent, debris extent, and debris thickness datasets.

Finally, we note that the parametric variance is considerable for all four models, indicating that accurate knowledge of local properties is crucial for energy balance modelling. For subdebris melt, the average parametric variance (here indicated by the inter-site mean of the standard deviation of melt rates for each site) exceeds the meteorological variance (indicated by the standard deviation of site mean melt rates) by a factor of two, due to the strong control of debris thickness. For ice cliffs, the parametric variance is equal to the meteorological variance due to the importance of cliff geometry. For both clean ice and supraglacial ponds, parametric variance is half the meteorological variance. Consequently, measuring debris properties is more important for accurate sub-debris melt rate estimation than precise local meteorology. Measuring ice cliff geometry, for example leveraging aerial, terrestrial, or satellite photogrammetry to produce high-resolution digital elevation models (Kraaijenbrink *et al* 2016, Watson *et al* 2017b, Brun *et al* 2018), is as important for estimating ice cliff melt as understanding local meteorology. On the other hand, an accurate representation of meteorological conditions is more important than local surface properties for estimating clean ice and supraglacial pond energy balance.

5. Conclusions

Our study used meteorological records collected over 13 debris-covered glacier sites around the world with four energy-balance models relevant to debris covered ice. Using Monte-Carlo simulations with meaningful distributions of physical parameters allowed us to disentangle the parametric and climatic drivers of melt rate and melt enhancement differences. Our key findings are that:

- Knowledge of site-specific physical parameters (debris thickness and thermal conductivity) is crucial for estimating sub-debris melt. However, assuming equivalent parameter distributions, the spatial variability in sub-debris melt rates is best explained by air temperature.
- Sub-debris melt rates are lower than clean ice and ice cliffs at all sites, and only six of thirteen sites exhibited a critical thickness. Given our empirical parameter distributions, sub-debris melt is generally one-tenth that of clean ice melt.
- Ice cliff melt is 2–3 times higher than clean ice at our study sites, but this melt enhancement is small when clean ice melt rates are already high. For a given location, ice cliff melt rates are most strongly controlled by geometry: radiative view factors, slope and aspect.
- The supraglacial pond net energy receipts are highly variable between sites, largely controlled by relative humidity and wind speed. The net energy

receipts for supraglacial ponds are very sensitive to water surface temperature (derived parametrically in our model), but are generally lower than clean ice in the equivalent setting, and are in some cases negative (evaporation-dominated).
- Climatic similarities between sites lead to distinctive regional patterns of melt rates and relative melt enhancement for each surface.
- We identify that variability in supraglacial pond and ice cliff melt rates and melt enhancement factors can be effectively parametrized independent of debris (relative to clean ice melt), and are directly related to meteorological conditions, but that physical parameters can lead to considerable differences between locations at any site.

Consequently, our results are promising for effective representation of ice cliffs and supraglacial ponds in larger-scale models. In particular, provided that regional distributions of cliffs and ponds are better known in the future, our study opens efficient approaches to estimate their melt rates and contribution to glacier-scale ablation regionally. However, our results also emphasize the need to account for site-specific physical parameters, which have a strong influence on modelled melt rates.

Data availability statement

The data that support the findings of this study are available upon reasonable request from the authors.

Acknowledgments

We are supremely grateful for the provision of automated weather station data for our study sites. In particular, we would like to thank the following data providers: Patrick Wagnon (Changri Nup, Lejeune *et al* 2013), the Direccion General de Aguas (DGA) and Centro de Estudios Cientificas (CECs) of Chile (Exploradores, unpublished), Yang Wei (24K, Yang *et al* 2017), Qiao Liu (Hailuogou, Zhang *et al* 2011), Lindsey Nicholson (Suldenferner, Nicholson 2019), Heather Purdie and Andrew Mackintosh (Tasman, Purdie 2019), the Glacial Party of Moscow State University (Djankuat AWS2, Rets *et al* 2019b), the Centro de Estudios Avanzados en Zonas Aridas (CEAZA) in Chile (Pirámide and Tapado, Ayala *et al* 2016, 2017). The views and interpretations in this publication are those of the authors and are not necessarily attributable to their organizations.

This project has received funding from the European Research Council (ERC) under the European Union's Horizon 2020 research and innovation program Grant Agreements No. 772751 (RAVEN, Rapid mass losses of debris-covered glaciers in High Mountain Asia). It has also been supported by the European Research Council (ERC) Grant Agreement 676819 (CAT, Climbing the Asian Water Tower). Pascal Buri greatly acknowledges financial and logistical support from M Truffer, A Aschwanden, J Fochesatto of the University of Alaska—Fairbanks and L Lajoie of the National Park Service, as well as project funding from the SNF Early Postdoc.Mobility program (Grant No. 178420). This research was further enabled by the data gathering and standardization efforts by the Debris Covered Glacier Working Group of the International Association of Cryospheric Scientists (IACS).

Appendix

Here we provide additional details about the meteorological stations and distinct model setups, and provide a summary table of the key results for each site. Model code and results are available on request from the authors.

Weather stations

Table 1. Summary of the on-glacier meteorological records used in this study.

Site	Name	Lon. (°)	Lat. (°)	Ele. (m.a.s.l.)	Model start	Model end	Reference	Notes
24K	24K	95.72	29.75	4000	1 June 2016	29 September 2016	Yang *et al* (2017), Fugger *et al* (2021)	
ARO	Arolla	7.52	45.98	2670	2 July 2010	9 September 2010	Carenzo *et al* (2016), Pellicciotti and Fontrodona Bach (2019)	
CNU	Changri Nup	86.79	27.99	5000	30 November 2014	21 November 2017	Sherpa *et al* (2017), Wagnon (2019), Fugger *et al* (2021)	
DJA	Djankuat	42.76	43.20	3050	22 July 2015	4 September 2015	Rets *et al* (2019a, 2019b)	
EXP	Exploradores	−73.19	−46.52	187	1 July 2015	31 December 2015	DGA-CECS	Patchy debris surface
HAI	Hailuogou	101.96	29.56	3550	14 May 2008	31 December 2008	Zhang *et al* (2011), Fugger *et al* (2021)	Air temperature lapsed from off-glacier station
KEN	Kennicott	−142.93	61.48	606	28 May 2019	22 August 2019	Buri *et al* (2022)	
LAN	Langtang	85.72	28.28	4600	11 May 2014	28 October 2014	Buri *et al* (2021)	
LIR	Lirung	85.56	28.24	4076	4 May 2014	24 October 2014	Pellicciotti *et al* (2019), Fugger *et al* (2021)	
MIA	Miage	6.88	45.78	2000	1 July 2010	4 September 2010	Carenzo *et al* (2016), Brock (2019)	
PIR	Piramide	−69.89	−33.59	3494	1 July 2014	30 June 2015	Ayala *et al* (2016), McPhee *et al* (2019)	
SUL	Suldenferner	10.57	46.50	2735	1 January 2016	31 December 2016	Nicholson (2019)	
TAP	Tapado	−69.93	−30.15	4775	1 July 2014	18 May 2015	Ayala *et al* (2017), MacPhee *et al* (2019)	
TAS	Tasman	−43.74	170.10	720	1 July 2017	1 July 2018	Purdie (2019)	

Energy balance models

We use established melt models to calculate the surface energy balance for a variety of glacier surface facies, always assuming that the glacier surface is snow-free (and in the ablation area) for each weather station. As the models have already been demonstrated, here we describe only the differences in model implementation from the studies in which they were established. For all models, we calculate the energy balance for a planimetric 1 m^2 patch of the surface as if directly situated beneath the meteorological station. For all model results, we report the resulting melt rate in water-equivalent (m w.e.).

Clean ice melt modelling

The melt rate for exposed, clean glacier ice is calculated using the clean-ice energy-balance model of Reid *et al* (2012), upon which the three other models herein have been developed. For consistency with those models, we assume that the surface is free of snow-cover and at the melting point. This is reasonable for most sites considering the relevant spatial and temporal domain (debris-covered ablation area during the ablation season), although ablation-season snowfall can modulate subsequent ablation (e.g. Fugger *et al* 2021). This model calculates the energy balance using *in situ* measurements of air temperature, relative humidity, wind speed, and incoming shortwave and longwave radiation, and requires parameters for ice albedo, roughness, and emissivity.

Sub-debris ice melt modelling

Sub-debris melt is calculated at the point scale with the model presented in detail in Steiner *et al* (2021). Incoming shortwave and longwave radiative fluxes are taken from measurements. Outgoing shortwave radiation is calculated with the prescribed albedo of the debris surface. Turbulent fluxes are calculated using the standard bulk approach. The model solves the flux through the debris iteratively at multiple layers of fixed thickness until surface temperature converges. This surface temperature is used for the calculation of outgoing longwave and sensible heat flux and is also used by the cliff model to derive longwave radiation emitted by the debris.

Ice cliff melt modelling

Ice cliff melt is calculated at the point scale, using measured station data of air temperature, relative humidity, wind speed, incoming short- and longwave radiation. Local shading is simulated based on slope and aspect of the cliff, assuming an even cliff shape and a constant horizon of 20 degrees for the far-topogaphy and determines the amount and timing of direct and diffuse shortwave radiation at the cliff surface. Viewing factors and emissivity values are taken from the parameter space and influence, together with the calculated surface temperature from the sub-debris ice melt model, the amount of longwave radiation emitted from the surrounding debris and received at the ice cliff surface. The model is described in detail in Buri *et al* (2016).

Supraglacial pond energy balance

The supraglacial pond energy balance is calculated at the point scale using the model of Miles *et al* (2018), which was developed specifically for meteorological measurements collected over debris (Miles *et al* 2016), using measured station data of air temperature, relative humidity, wind speed, incoming shortwave and longwave radiation. The parametrization for water surface temperature has been established based on contemporaneous water surface and air temperature measurements (Miles *et al* 2018). For this implementation, we do not perform a sky view correction based on nearby topography. Consequently, six parameters are needed for this model: three parameters to estimate water surface temperature, as well as an estimate of water surface roughness, broadband albedo, and emissivity.

Energy balance physical parameters

The key parameters specified for each model, including the probability distribution of values, is depicted in table 2. The probability distributions were derived based on available literature, and were used to derive 5000 randomly-sample model realizations.

Summary of results

Table 2. Summary of parameter distributions used in the 5000 model realizations.

Parameter	Name	Model	References	Distribution Type	Param1	Val1	Param2	Val2
d	Debris thickness	Debris	McCarthy *et al* (2017), Nicholson and Mertes (2017), Nicholson *et al* (2018)	Weibull	alpha	2	beta	1
k_d	Debris thermal conductivity	Debris	Nicholson and Benn (2012), Rounce *et al* (2015)	uniform	min	0.465	max	2
$z_{0,d}$	Debris surface roughness	Debris	Miles *et al* (2017b)	log-uniform	min	0.001	max	0.06
α_d	Debris albedo	Debris	Nicholson and Benn (2012), Rounce *et al* (2015)	normal	mean	0.25	sigma	0.05
ϵ_d	Debris emissivity	Debris	Steiner *et al* (2015)	uniform	min	0.94	max	0.95
ϕ_d	Debris porosity	Debris	Reid and Brock (2014)	normal	mean	0.29	sigma	0.01
ρ_r	Rock density	Debris	Reid and Brock (2014)	normal	mean	2650	sigma	300
c_d	Debris specific heat capacity	Debris	Reid and Brock (2014)	uniform	min	850	max	1045
$z_{0,i}$	Ice cliff surface roughness	Cliff	Steiner *et al* (2015)	log-uniform	min	0.001	max	0.005
α_i	Ice cliff albedo	Cliff	Steiner *et al* (2015)	uniform	min	0.01	max	0.35
ϵ_i	Ice cliff emissivity	Cliff, clean	Steiner *et al* (2015)	uniform	min	0.95	max	0.99
ψ_i	Ice cliff aspect	Cliff	Buri and Pellicciotti (2018)	uniform	range	0–360	increment	45
i	Ice cliff Surface slope	Cliff	Buri *et al* (2016), Herreid and Pellicciotti (2018)	uniform	min	35	max	60
$T_{ws,0}$	Baseline value of T_{ws}	Pond	Miles *et al* (2018)	uniform	min	0	max	3.5
$T_{ws,a}$	Ratio of diurnal anomalies in T_{ws} vs T_a	Pond	Miles *et al* (2018)	normal	mean	0.178	sigma	0.006
$T_{ws,m}$	Ratio of mean anomalies of T_{ws} vs T_a	Pond	Miles *et al* (2018)	normal	mean	0.085	sigma	0.005
$z_{0,p}$	Pond surface roughness	Pond	Miles *et al* (2018)	log-uniform	min	0.00002	max	0.002
α_p	Pond albedo	Pond	Miles *et al* (2018)	uniform	min	0.04	max	0.16
w	Pond emissivity	Pond	Miles *et al* (2018)	uniform	min	0.95	max	0.96
$z_{0,g}$	Glacier surface roughness	Clean	Brock *et al* (2006)	log-uniform	min	0.0001	max	0.005
α_g	Glacier albedo, ablation area	Clean	Cuffey and Paterson (2010)	uniform	min	0.2	max	0.65
$V_{s,I}$	Shortwave sky view factor	Cliff	Han *et al* (2010), Reid and Brock (2014), Steiner *et al* (2015)	uniform	min	0.67	max	0.8
$V_{s,L}$	Longwave sky view factor	Cliff	Han *et al* (2010), Reid and Brock (2014), Steiner *et al* (2015)	uniform	min	0.83	max	1.03
V_d	Debris view factor	Cliff	Han *et al* (2010), Reid and Brock (2014), Steiner *et al* (2015)	uniform	min	0.39	max	0.57

Table 3. Key results for each site, including the mean modelled melt rate for each surface (μ) and its variability (σ). Also shown are fitted Østrem curve parameters for sub-debris melt rates according to the rational form $y = \frac{p}{x+q}$, and critical debris thicknesses (also depicting confidence interval) for the Østrem curves considering the site's clean-ice melt rate. Glacier labels: 24K—24K, ARO—Arolla, CNU—Changri Nup, DJA—Djankuat, EXP—Exploradores, HAI—Hailuogou, KEN—Kennicott, LIR—Lirung, MIA—Miage, PIR—Piramide, SUL—Suldenferner, TAP—Tapado, TAS—Tasman.

	Mean melt rates (m w.e. d^{-1})								Østrem parameters		Critical thicknesses (m)		
Site	Debris μ	Debris σ	Cliff μ	Cliff σ	Pond μ	Pond σ	Clean μ	Clean σ	p (d^{-1})	q (m)	0.975 CI	Best-fit	0.025 CI
24K	0.010	0.0092	0.13	0.023	0.076	0.017	0.059	0.008	0.0062	0.1019	—	—	0.026
ARO	0.0050	0.0046	0.10	0.020	0.016	0.015	0.041	0.008	0.0028	0.0562	—	0.013	0.035
CNU	0.0049	0.0044	0.91	0.017	0.073	0.025	0.093	0.034	0.0031	0.0883	—	—	—
DJA	0.0075	0.0071	0.16	0.029	0.018	0.018	0.082	0.012	0.0041	0.0503	—	—	0.010
EXP	0.0014	0.0016	0.091	0.014	0.035	0.020	0.034	0.002	0.0010	0.0323	—	—	—
HAI	0.0074	0.0063	0.095	0.016	0.057	0.014	0.036	0.005	0.0043	0.0875	0.013	0.031	0.057
KEN	0.012	0.0099	0.12	0.023	0.040	0.025	0.089	0.010	0.0074	0.1431	—	—	—
LIR	0.0089	0.0073	0.10	0.020	0.053	0.0061	0.040	0.009	0.0055	0.1362	—	—	0.052
MIA	0.011	0.0099	0.13	0.023	0.042	0.024	0.058	0.009	0.0058	0.0595	0.024	0.041	0.065
PIR	0.0071	0.0066	0.12	0.025	0.0000	0.0000	0.047	0.012	0.0039	0.0597	—	0.024	0.058
SUL	0.0044	0.0042	0.091	0.018	0.021	0.011	0.032	0.009	0.0027	0.0654	—	0.018	0.054
TAP	0.0032	0.0033	0.092	0.022	0.0000	0.0000	0.023	0.009	0.0036	0.2177	—	—	0.073
TAS	0.0071	0.0067	0.093	0.017	0.011	0.0077	0.029	0.002	0.0039	0.0509	0.077	0.085	0.10

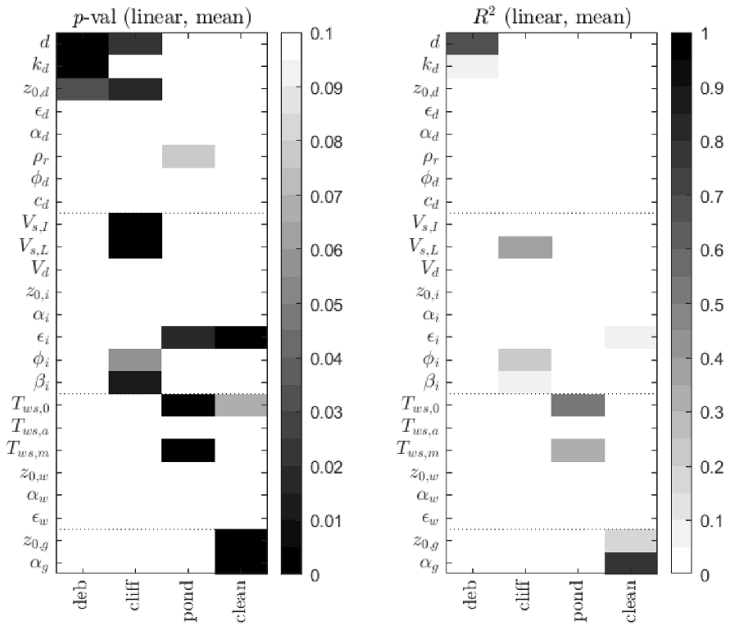

Figure 6. Mean p-value (left) and R^2 (right) for correlations between melt rates and individual parameters at each site. Selected parameters were modified by $log(x)$ (for d, all z_0) or $sin(x)$ (for ϕ_i) before correlation.

ORCID iDs

E S Miles https://orcid.org/0000-0001-5446-8571
J F Steiner https://orcid.org/0000-0002-0063-0067
P Buri https://orcid.org/0000-0003-3890-2109
W W Immerzeel https://orcid.org/0000-0002-2010-9543
F Pellicciotti https://orcid.org/0000-0002-5554-8087

References

Anderson L S and Anderson R S 2016 Modeling debris-covered glaciers: response to steady debris deposition *The Cryosphere* **10** 1105–24

Anderson L, Armstrong W, Anderson R and Buri P 2021 Debris cover and the thinning of Kennicott Glacier, Alaska: *in situ* measurements, automated ice cliff delineation and distributed melt estimates *The Cryosphere* **15** 265–82

Ayala A, Pellicciotti F, MacDonell S, McPhee J and Burlando P 2017 Patterns of glacier ablation across North-Central Chile: identifying the limits of empirical melt models under sublimation-favorable conditions *Water Resour. Res.* **53** 5601–25

Ayala A, Pellicciotti F, Macdonell S, Mcphee J, Vivero S, Campos C and Egli P 2016 Modelling the hydrological response of debris-free and debris-covered glaciers to present climatic conditions in the semiarid Andes of central Chile *Hydrol. Process.* **4058** 4036–58

Benn D I, Wiseman S and Hands K A 2001 Growth and drainage of supraglacial lakes on debris-mantled Ngozumpa Glacier, Khumbu Himal, Nepal *J. Glaciol.* **47** 626–38

Benn D, Bolch T, Hands K, Gulley J, Luckman A, Nicholson L, Quincey D, Thompson S, Toumi R and Wiseman S 2012 Response of debris-covered glaciers in the Mount Everest region to recent warming and implications for outburst flood hazards *Earth-Sci. Rev.* **114** 156–74

Braithwaite R J 1981 On glacier energy balance, ablation and air temperature *J. Glaciol.* **27** 381–91

Brock B W 2019 5_Miage Data (https://doi.org/10.5281/zenodo.3050557)

Brock B W, Willis I C and Sharp M J 2006 Measurement and parameterization of aerodynamic roughness length variations at Haut Glacier d'Arolla, Switzerland *J. Glaciol.* **52** 281–97

Brun F, Buri P, Miles E S, Wagnon P, Steiner J F, Berthier E, Ragettli S, Kraaijenbrink P, Immerzeel W W and Pellicciotti F 2016 Quantifying volume loss from ice cliffs on debris-covered glaciers using high resolution terrestrial and aerial photogrammetry *J. Glaciol.* **62** 684–95

Brun F, Wagnon P, Berthier E, Shea J M, Immerzeel W W, Kraaijenbrink P D A, Vincent C, Reverchon C, Shrestha D and Arnaud Y 2018 Ice cliff contribution to the tongue-wide ablation of Changri Nup Glacier, Nepal, central Himalaya *The Cryosphere* **12** 3439–57

Buri P, Miles E S, Steiner J F, Ragettli S and Pellicciotti F 2021 Supraglacial ice cliffs can substantially alter the mass balance of debris-covered glaciers *Geophys. Res. Lett.* **48** e2020GL092150

Buri P and Pellicciotti F 2018 Aspect controls the survival of ice cliffs on debris-covered glaciers *Proc. Natl Acad. Sci.* **115** 4369–74

Buri P, Pellicciotti F, Steiner J F, Miles E S and Immerzeel W W 2016 A grid-based model of backwasting of supraglacial ice cliffs on debris-covered glaciers *Ann. Glaciol.* **57** 199–211

Buri P, Truffer M, Fochesatto J and Aschwanden A 2022 Automatic weather station data from the debris-covered Kennicott Glacier, Alaska (May–Aug 2019) (https://doi.org/10.5281/ZENODO.6424158)

Carenzo M, Pellicciotti F, Mabillard J, Reid T and Brock B W 2016 An enhanced debris temperature index model accounting for thickness effect *Adv. Water Resour.* **94** 457–69

Compagno L, Huss M, Miles E S, McCarthy M J, Zekollari H, Pellicciotti F and Farinotti D 2021 Modelling supraglacial debris-cover evolution from the single glacier to the regional scale: an application to High Mountain Asia *The Cryosphere* in review (https://doi.org/10.5194/tc-2021-233)

Cuffey K M and Paterson W 2010 *The Physics of Glaciers* 4th edn (Amsterdam: Elsevier) p 704

Evatt G W, Abrahams I D, Heil M, Kingslake J, Mitchell S L, Andrew C and Clark C D 2015 Glacial melt under a porous debris layer *J. Glaciol.* **61** 825–36

Falaschi D, Rivera A, Lo Vecchio Repetto A, Moragues S, Villalba R, Rastner P, Zeller J and Salcedo A P 2021 Evolution of surface characteristics of three debris-covered glaciers in the Patagonian Andes From 1958 to 2020 *Frontiers Earth Sci.* **9** 1–19

Ferguson J C and Vieli A 2021 Modelling steady states and the transient response of debris-covered glaciers *The Cryosphere* **15** 3377–99

Fick S E and Hijmans R J 2017 WorldClim 2: new 1-km spatial resolution climate surfaces for global land areas *Int. J. Climatol.* **37** 4302–15

Fugger S *et al* 2021 Understanding monsoon controls on the energy and mass balance of Himalayan glaciers *The Cryosphere* in press (https://doi.org/10.5194/tc-2021-97)

Fyffe C L, Woodget A S, Kirkbride M P, Deline P, Westoby M J and Brock B W 2020 Processes at the margins of supraglacial debris cover: quantifying dirty ice ablation and debris redistribution *Earth Surf. Process. Landf.* **45** 2272-90

Gardelle J, Arnaud Y and Berthier E 2011 Contrasted evolution of glacial lakes along the Hindu Kush Himalaya mountain range between 1990 and 2009 *Glob. Planet. Change* **75** 47–55

Han H, Wang J, Wei J and Liu S 2010 Backwasting rate on debris-covered Koxkar glacier, Tuomuer mountain, China *J. Glaciol.* **56** 287–96

Herreid S and Pellicciotti F 2018 Automated detection of ice cliffs within supraglacial debris cover *The Cryosphere* **12** 1811–29

Herreid S and Pellicciotti F 2020 The state of rock debris covering Earth's glaciers *Nat. Geosci.* **13** 621–7

Hock R 2005 Glacier melt and discharge: a review on processes and their modelling *Prog. Phys. Geogr.* **29** 362–91

Huss M and Hock R 2015 A new model for global glacier change and sea-level rise *Frontiers Earth Sci.* **3** 1–22

Immerzeel W, Kraaijenbrink P, Shea J, Shrestha A, Pellicciotti F, Bierkens M and de Jong S 2014 High-resolution monitoring of Himalayan glacier dynamics using unmanned aerial vehicles *Remote Sens. Environ.* **150** 93–103

King O, Turner A G, Quincey D J and Carrivick J L 2020 Morphometric evolution of Everest region debris-covered glaciers *Geomorphology* **371** 107422

Kneib M, Miles E S, Buri P, Molnar P, McCarthy M, Fugger S and Pellicciotti F 2021b Interannual dynamics of ice cliff populations on debris-covered glaciers from remote sensing observations and stochastic modeling *J. Geophys. Res.: Earth Surf.* **126** e2021JF006179

Kneib M, Miles E, Jola S, Buri P, Herreid S, Bhattacharya A, Watson C, Bolch T, Quincey D and Pellicciotti F 2021a Mapping ice cliffs on debris-covered glaciers using multispectral satellite images *Remote Sens. Environ.* **253** 112201

Kraaijenbrink P D A, Shea J M, Pellicciotti F, Jong S M D and Immerzeel W W 2016 Object-based analysis of unmanned aerial vehicle imagery to map and characterise surface features on a debris-covered glacier *Remote Sens. Environ.* **186** 581–95

Kraaijenbrink P D, Bierkens M F, Lutz A F and Immerzeel W W 2017 Impact of a global temperature rise of 1.5 degrees Celsius on Asia's glaciers *Nature* **549** 257–60

Lejeune Y, Bertrand J M, Wagnon P and Morin S 2013 A physically based model of the year-round surface energy and mass balance of debris-covered glaciers *J. Glaciol.* **59** 327–44

MacPhee J, Ayala A and MacDonell S 2019 8_Tapado Data (https://doi.org/10.5281/ZENODO.3362402)

Marzeion B *et al* 2020 Partitioning the uncertainty of ensemble projections of global glacier mass change *Earth's Future* **8** e2019EF001470

McCarthy M, Pritchard H, Willis I and King E 2017 Ground-penetrating radar measurements of debris thickness on Lirung Glacier, Nepal *J. Glaciol.* **63** 1–13

McPhee J, MacDonell S and Shaw T 2019 6_Pirámide Data (https://doi.org/10.5281/zenodo.3056072)

Miles E S, Pellicciotti F, Willis I C, Steiner J F, Buri P and Arnold N S 2016 Refined energy-balance modelling of a supraglacial pond, Langtang Khola, Nepal *Ann. Glaciol.* **57** 29–40

Miles E S, Steiner J F and Brun F 2017b Highly variable aerodynamic roughness length (z_0) for a hummocky debris-covered glacier *J. Geophys. Res.: Atmos.* **122** 8447–66

Miles E S, Steiner J, Willis I C, Buri P, Immerzeel W W, Chesnokova A and Pellicciotti F 2017a Pond dynamics and supraglacial-englacial connectivity on debris-covered Lirung Glacier, Nepal *Frontiers Earth Sci.* **5** 1–19

Miles E S, Willis I C, Arnold N S, Steiner J F and Pellicciotti F 2017c Spatial, seasonal and interannual variability of supraglacial ponds in the Langtang Valley of Nepal, 1999 to 2013 *J. Glaciol.* **63** 88–105

Miles E S, Willis I, Pellicciotti F, Buri P, Steiner J F and Arnold N S 2018 Surface pond energy absorption across four Himalayan glaciers accounts for 1/8 of total catchment ice loss *Geophys. Res. Lett.* **45** 10464–73

Mishra N B, Miles E S, Chaudhuri G, Mainali K P, Mal S, Singh P B and Tiruwa B 2021 Quantifying heterogeneous monsoonal melt on a debris-covered glacier in Nepal Himalaya using repeat uncrewed aerial system (UAS) photogrammetry *J. Glaciol.* **68** 288–304

Mölg N, Bolch T, Walter A and Vieli A 2019 Unravelling the evolution of Zmuttgletscher and its debris cover since the end of the little ice age *The Cryosphere* **13** 1889–909

Nicholson L I, McCarthy M, Pritchard H D and Willis I 2018 Supraglacial debris thickness variability: Impact on ablation and relation to terrain properties *The Cryosphere* **12** 3719–34

Nicholson L 2019 7_Suldenferner Data (https://doi.org/10.5281/zenodo.3056524)

Nicholson L and Benn D I 2006 Calculating ice melt beneath a debris layer using meteorological data *J. Glaciol.* **52** 463–70

Nicholson L and Benn D I 2013 Properties of natural supraglacial debris in relation to modelling sub-debris ice ablation *Earth Surf. Process. Landf.* **38** 490–501

Nicholson L and Mertes J 2017 Thickness estimation of supraglacial debris above ice cliff exposures using a high-resolution digital surface model derived from terrestrial photography *J. Glaciol.* **63** 989–98

Nicholson L and Stiperski I 2020 Comparison of turbulent structures and energy fluxes over exposed and debris-covered glacier ice *J. Glaciol.* **66** 543–55

Östrem G 1959 Ice melting under a thin layer of moraine and the existence of ice cores in moraine ridges *Geografiska Ann.* **41** 228–30

Pellicciotti F, Brock B, Strasser U, Burlando P, Funk M and Corripio J 2005 An enhanced temperature-index glacier melt model including the shortwave radiation balance: Development and testing for Haut Glacier d'Arolla, Switzerland *J. Glaciol.* **51** 573–87

Pellicciotti F and Fontrodona Bach A 2019 1_Arolla Data (https://doi.org/10.5281/ZENODO.3047649)

Pellicciotti F, Fugger S and Miles E 2019 4_Lirung Data (https://doi.org/10.5281/ZENODO.3050327)

Pellicciotti F, Stephan C, Miles E, Herreid S, Immerzeel W W and Bolch T 2015 Mass-balance changes of the debris-covered glaciers in the Langtang Himal, Nepal, 1974–99 *J. Glaciol.* **61** 1–14

Pfeffer W T *et al* (The Randolph Consortium) 2014 The Randolph Glacier Inventory: a globally complete inventory of glaciers *J. Glaciol.* **60** 537–52

Pourrier J, Jourde H, Kinnard C, Gascoin S and Monnier S 2014 Glacier meltwater flow paths and storage in a geomorphologically complex glacial foreland: the case of the Tapado glacier, dry Andes of Chile (30° S) *J. Hydrol.* **519** 1068–83

Purdie H 2019 9_Tasman Data (https://doi.org/10.5281/zenodo.3354105)

Radić V, Bliss A, Beedlow A C, Hock R, Miles E and Cogley J G 2014 Regional and global projections of twenty-first century glacier mass changes in response to climate scenarios from global climate models *Clim. Dyn.* **42** 37–58

Reid T D, Carenzo M, Pellicciotti F and Brock B W 2012 Including debris cover effects in a distributed model of glacier ablation *J. Geophys. Res.* **117(D18)** 1–15
Reid T and Brock B 2014 Assessing ice-cliff backwasting and its contribution to total ablation of debris-covered Miage glacier, Mont Blanc massif, Italy *J. Glaciol.* **60** 3–13
Rets E P *et al* 2019b Djankuat glacier station in the North Caucasus, Russia: a database of glaciological, hydrological and meteorological observations and stable isotope sampling results during 2007–2017 *Earth Syst. Sci. Data* **11** 1463–81
Rets E, Popovnin V and Shahgedanova M 2019a 3_Djankuat Data (https://doi.org/10.5281/ZENODO.3049871)
Reznichenko N, Davies T, Shulmeister J and McSaveney M 2010 Effects of debris on ice-surface melting rates: an experimental study *J. Glaciol.* **56** 384–94
Röhl K 2006 Thermo-erosional notch development at fresh-water-calving Tasman Glacier, New Zealand *J. Glaciol.* **52** 203–13
Röhl K 2008 Characteristics and evolution of supraglacial ponds on debris-covered Tasman Glacier, New Zealand *J. Glaciol.* **54** 867–80
Rounce D R *et al* 2021 Distributed global debris thickness estimates reveal debris significantly impacts glacier mass balance *Geophys. Res. Lett.* **48** e2020GL091311
Rounce D R, Quincey D J and McKinney D C 2015 Debris-covered glacier energy balance model for Imja–Lhotse Shar Glacier in the Everest region of Nepal *The Cryosphere* **9** 1–16
Rowan A V, Egholm D L, Quincey D J, Hubbard B, King O, Miles E S, Miles K E and Hornsey J 2021 The role of differential ablation and dynamic detachment in driving accelerating mass loss from a debris-covered Himalayan glacier *J. Geophys. Res.: Earth Surf.* **126** e2020JF005761
Sakai A, Nakawo M and Fujita K 1998 Melt rate of ice cliffs on the Lirung Glacier, Nepal Himalayas, 1996 *Bull. Glacier Res.* **16** 57–66
Sakai A, Nakawo M and Fujita K 2002 Distribution characteristics and energy balance of ice cliffs on debris-covered glaciers, Nepal Himalaya *Arctic, Antarct. Alpine Res.* **34** 12
Sakai A, Takeuchi N, Fujita K and Nakawo M 2000 Role of supraglacial ponds in the ablation process of a debris-covered glacier in the Nepal Himalayas *Seattle Symposium, 2000, Debris-Covered Glaciers, IAHS Publ. No 264*, ed M Nakawo, C F Raymond and A Fountain (IAHS) pp 119–30
Salerno F, Thakuri S, Fujita K and Nuimura T 2017 Debris-covered glacier anomaly? Morphological factors controlling changes in mass balance, surface area, terminus position and snow line altitude of Himalayan glaciers *Earth Planet. Sci. Lett.* **471** 19–31
Scherler D, Wulf H and Gorelick N 2018 Global assessment of supraglacial debris-cover extents *Geophys. Res. Lett.* **45** 11798–805
Shaw T E, Brock B W, Ayala A, Rutter N and Pellicciotti F 2017 Centreline and cross-glacier air temperature variability on an Alpine glacier: assessing temperature distribution methods and their influence on melt model calculations *J. Glaciol.* **6** 973–88
Sherpa S F, Wagnon P, Brun F, Berthier E, Vincent C, Lejeune Y, Arnaud Y, Kayastha R B and Sinisalo A 2017 Contrasted surface mass balances of debris-free glaciers observed between the southern and the inner parts of the Everest region (2007–15) *J. Glaciol.* **63** 637–51
Stefaniak A M, Robson B A, Cook S J, Clutterbuck B, Midgley N G and Labadz J C 2021 Mass balance and surface evolution of the debris-covered Miage Glacier, 1990–2018 *Geomorphology* **373** 107474
Steiner J F, Buri P, Miles E S, Ragettli S and Pellicciotti F 2019 Supraglacial ice cliffs and ponds on debris-covered glaciers: spatio-temporal distribution and characteristics *J. Glaciol.* **65** 617–32
Steiner J F, Kraaijenbrink P D A and Immerzeel W W 2021 Distributed melt on a debris-covered glacier: field observations and melt modelling on the Lirung Glacier in the Himalaya *Frontiers Earth Sci.* **9** 1–38
Steiner J F, Litt M, Stigter E E, Shea J, Bierkens M F P and Immerzeel W W 2018 The importance of turbulent fluxes in the surface energy balance of a debris-covered glacier in the Himalayas *Frontiers Earth Sci.* **6** 1–18
Steiner J F, Pellicciotti F, Buri P, Miles E S, Immerzeel W W and Reid T D 2015 Modelling ice-cliff backwasting on a debris-covered glacier in the Nepalese Himalaya *J. Glaciol.* **61** 889–907
Steiner J and Pellicciotti F 2016 Variability of air temperature over a debris-covered glacier in the Nepalese Himalaya *Ann. Glaciol.* **57** 295–307
Thompson S, Benn D I, Mertes J and Luckman A 2016 Stagnation and mass loss on a Himalayan debris-covered glacier: processes, patterns and rates *J. Glaciol.* **62** 467–85
Wagnon P 2019 2_Changri Nup Data (https://doi.org/10.5281/ZENODO.3048780)
Watson C S, King O, Miles E S and Quincey D J 2018 Optimising NDWI supraglacial pond classification on Himalayan debris-covered glaciers *Remote Sens. Environ.* **217** 414–25
Watson C S, Quincey D J, Carrivick J L, Smith M W, Rowan A V and Richardson R 2017a Heterogeneous water storage and thermal regime of supraglacial ponds on debris-covered glaciers *Earth Surf. Process. Landf.* **43** 229–41
Watson C S, Quincey D J, Smith M W, Carrivick J L, Rowan A V and James M R 2017b Quantifying ice cliff evolution with multi-temporal point clouds on the debris-covered Khumbu Glacier, Nepal *J. Glaciol.* **63** 823–37
Watson C, Quincey D, Carrivick J and Smith M 2016 The dynamics of supraglacial ponds in the Everest region, central Himalaya *Glob. Planet. Change* **142** 14–27
Xin W, Shiyin L, Han H, Jian W and Qiao L 2012 Thermal regime of a supraglacial lake on the debris-covered Koxkar Glacier, southwest Tianshan, China *Environ. Earth Sci.* **67** 175–83
Yang W, Yao T, Zhu M and Wang Y 2017 Comparison of the meteorology and surface energy fluxes of debris-free and debris-covered glaciers in the southeastern Tibetan Plateau *J. Glaciol.* **63** 1090–104
Zhang Y, Fujita K, Liu S, Liu Q and Nuimura T 2011 Distribution of debris thickness and its effect on ice melt at Hailuogou glacier, southeastern Tibetan Plateau, using *in situ* surveys and ASTER imagery *J. Glaciol.* **57** 1147–57